

# The structure of compositionally constrained zinc-ferrite spinel nanoparticles

Darko Makovec · Alojz Kodre · Iztok Arčon ·  
Miha Drofenik

Received: 13 December 2009 / Accepted: 9 April 2010 / Published online: 24 April 2010  
© Springer Science+Business Media B.V. 2010

**Abstract**  $\text{ZnFe}_2\text{O}_4$  bulk material shows a normal-spinel structure and a closely defined composition at  $\text{Zn}^{2+}/\text{Fe}^{3+} \cong 0.5$ . However, the composition of zinc ferrite, prepared as nanoparticles, can be varied in a broad range without losing the single-phase spinel structure. In this article, structural mechanisms enabling this non-stoichiometry were studied using the X-ray absorption fine structure (EXAFS) in combination with X-ray diffractometry (XRD), transmission electron microscopy (TEM), and magnetic measurements. Nanoparticles with a narrow size distribution were synthesized using co-precipitation in water-in-oil microemulsions. First, the structure of the stoichiometric zinc-ferrite nanoparticles was studied in dependence of their size and the annealing

temperature. EXAFS analysis showed that the degree of inversion  $x$  (as defined in the compound formula  $(\text{Zn}_{1-x}\text{Fe}_x)[\text{Fe}_{2-x}\text{Zn}_x]\text{O}_4$ , with round and square brackets representing the tetrahedral and octahedral sites, respectively) increased with decreasing nanoparticles size. The structure of the stoichiometric nanoparticles and the nanoparticles of comparable size displaying Zn/Fe ratio of 0.2 (Fe-rich) and 0.7 (Zn-rich) were then compared. Analysis showed that the non-stoichiometry is structurally compensated predominantly in the core of the nanoparticle by the adjusted distribution of Zn and Fe ions over the two sublattices of the spinel structure.

**Keywords** Magnetic nanoparticles · Stoichiometry · EXAFS · Spinel · Size effect · Particle synthesis in microemulsion

**Electronic supplementary material** The online version of this article (doi:[10.1007/s11051-010-9929-y](https://doi.org/10.1007/s11051-010-9929-y)) contains supplementary material, which is available to authorized users.

D. Makovec (✉) · A. Kodre · I. Arčon · M. Drofenik  
Jožef Stefan Institute, Ljubljana, Slovenia  
e-mail: Darko.Makovec@ijs.si

A. Kodre  
Faculty of Mathematics and Physics, University  
of Ljubljana, Ljubljana, Slovenia

I. Arčon  
University of Nova Gorica, Nova Gorica, Slovenia

M. Drofenik  
Faculty for Chemistry and Chemical Engineering,  
University of Maribor, Maribor, Slovenia

## Introduction

Zinc ferrite is a good example of the direct relation between the nanoparticle structure, composition, and properties. When prepared as a bulk material,  $\text{ZnFe}_2\text{O}_4$  has a normal-spinel structure with  $\text{Zn}^{2+}$  incorporated almost exclusively at the tetrahedral A lattice sites and  $\text{Fe}^{3+}$  at the octahedral B-sites of the  $\text{AB}_2\text{O}_4$  spinel lattice (Ligenza 1976; O'Neill 1992). Since the A-sublattice is almost exclusively populated by the non-magnetic zinc atoms, zinc-ferrite bulk material is paramagnetic at room temperature (Lotgering 1966; Brockhouse et al. 1955). When

prepared as the nanoparticles, however, zinc ferrite turns ferrimagnetic. The ferrimagnetism of the zinc-ferrite nanoparticles was explained by incorporation of a significant proportion of Zn atoms at the octahedral B-sites (Sato et al. 1990; Kamiyama et al. 1992; Jeyadevan et al. 1994; Hamdeh et al. 1997; Ammar et al. 2004). The degree of inversion depends strongly on the method of synthesis (Hamdeh et al. 1997; Ammar et al. 2004); however, it generally increases with decreasing particle size (Kamiyama et al. 1992). When the nanoparticles are exposed to elevated temperatures their structure rearranges to approach the bulk structure (Hamdeh et al. 1997; Makovec and Drofenik 2008). Changing of the lattice parameter of the  $\text{ZnFe}_2\text{O}_4$  nanoparticles with annealing temperature suggested a quite abrupt rearrangement of the structure around the temperature of 260 °C; i.e., before the nanoparticles started to grow (an exponential increase of the particles size was observed above approximately 300 °C). The decrease of the magnetization of the nanoparticles with temperature was more gradual, starting above approximately 200 °C and reaching the bulk value at approximately 450 °C (Makovec and Drofenik 2008).

The “rigid” structure of bulk zinc ferrite characterized by the large affinity of Zn for the tetrahedral lattice sites also maintains its composition at  $\text{Zn}^{2+}/\text{Fe}^{3+} \cong 0.5$ . In the reducing conditions stabilizing  $\text{Fe}^{2+}$ , zinc ferrite forms a complete solid solution with  $\text{Fe}_3\text{O}_4$  (Lykasov et al. 1991). In air, however, the solid solubility of  $\text{Fe}_2\text{O}_3$  in  $\text{ZnFe}_2\text{O}_4$  strongly depends on temperature. At low temperatures it is very limited, below 2 mol% at 800 °C (Mason 1947; Tanida and Kitamura 1984). Whereas a limited solubility of Fe oxide is possible, a significant amount of  $\text{ZnO}$  cannot be dissolved in the zinc-ferrite spinel lattice above its stoichiometric  $\text{ZnFe}_2\text{O}_4$  composition. However, when zinc ferrite is prepared in the form of the nanoparticles, it shows a large flexibility of its composition. In our previous article (Makovec and Drofenik 2008), we showed that the zinc-ferrite nanoparticles with a size of ~8 nm retained the single-phase spinel structure for Zn/Fe molar ratio in the range between 0 and ~0.8. With a decrease in the particle size, the compositional range of the zinc-ferrite spinel broadened. The rearrangement of the structure of the non-stoichiometric nanoparticles at elevated temperatures resulted in a shift of their composition toward the stoichiometric

and, as the result, in the precipitation of the excess  $\text{ZnO}$  or  $\text{Fe}_2\text{O}_3$ .

We believe that the flexibility of the composition observed in the zinc-ferrite nanoparticles is a general property of the nanoparticles of numerous mixed oxides. It can be applied for the synthesis of the nanoparticles displaying new properties, not observed in the corresponding bulk materials.

The synthesis of the nanoparticles with the composition significantly different from that of the bulk material poses a question, how the non-stoichiometry is structurally accommodated? In order to get insight into the type of deviations of the structure of the nanoparticles from that of the bulk, in this study the structure of non-stoichiometric nanoparticles has been studied by a combination of classical macroscopic methods and extended X-ray absorption fine structure (EXAFS). The structure of the non-stoichiometric nanoparticles was compared to that of the stoichiometric nanoparticles of different sizes and the nanoparticles heated at elevated temperatures, whereby their structure approached the “bulk” state.

## Experimental

Zinc-ferrite nanoparticles with different Zn-to-Fe atom ratios of 0.71 (sample ZF0.7-8), 0.5 (samples ZF0.5-3 and ZF0.5-8) and 0.2 (ZF0.2-8) were synthesized using the co-precipitation in an environment of inverse microemulsions. Table 1 lists the basic properties of the synthesized nanoparticles. The synthesis procedure is described in detail in reference Makovec and Drofenik (2008). In brief, the two microemulsions consisting of an aqueous phase (15 wt% for a sample ZF0.5-3, and 30 wt% for all other samples), n-hexanol as the oil phase (15 wt%), n-hexadecyl trimethylammonium bromide (CTAB) as the surfactant and butanol as the co-surfactant (the weight ratio CTAB/butanol = 1.5) were mixed. The aqueous phase of the microemulsion  $\mu\text{EA}$  contained a solution of  $\text{Zn}^{2+}$  and  $\text{Fe}^{2+}$ -sulfates (a total concentration of metal ions of 0.125 mol/L for the sample ZF0.5-3 and 0.25 mol/L for all other samples), and the microemulsion  $\mu\text{EB}$  contained a solution of the precipitating agent tetramethyl ammonium hydroxide (0.5 mol/L). The amount of  $\mu\text{EB}$  was set to a value that resulted in a final pH after the precipitation of more than 12.5. After the precipitation of the metal ions, the reaction mixture

**Table 1** Properties of the nanoparticles

Sample code	Zn/Fe ratio (-)	Annealing temperature (°C)	Particle size <sup>a</sup> (nm)	$M_S^b$ (emu/g)	Lattice parameter(nm)
ZF0.2-8	0.20	—	7.9	22.3	0.84164(12)
ZF0.7-8	0.71	—	8.5	2.4	0.84804(12)
ZF0.5-3	0.50	—	3.2	4.0	—
ZF0.5-8	0.50	—	8.8	5.4	0.84562(12)
ZF0.5-180	0.50	180	8.8	5.4	0.84579(12)
ZF0.5-405	0.50	405	13.7	1.8	0.84410(8)
ZF0.5-500	0.50	500	24.2	1.6	0.84406(6)

<sup>a</sup> Particle size determined from XRD peak broadening

<sup>b</sup> Specific magnetization measured at 10 kOe

was aged for 1 h with mixing in ambient air to allow the oxidation of  $\text{Fe}^{2+}$ , resulting in the formation of the spinel product. During the synthesis, the temperature was maintained at 50 °C. Finally, the product nanoparticles were washed with ethanol and dried in ambient air at 70 °C.

In order to evaluate the influence of elevated temperatures on the structure, the nanoparticles ZF0.5-8 were annealed in air for 16 h at 180 °C (sample ZF0.5-180), 405 °C (ZF0.5-405) and 500 °C (ZF0.5-500).

The nanoparticles were characterized using X-ray powder diffractometry (XRD) (Model D4 Endeavor, Bruker AXS, Cu K $\alpha$  X-ray source) and by transmission electron microscopy (TEM) (JEOL 2010 F field-emission TEM). For the TEM investigations, the nanoparticles were deposited on a copper-grid-supported transparent carbon foil.

The composition of the nanoparticles was checked by energy dispersive EDX analysis in TEM and by dissolving the nanoparticles in HCl and analyzing the solution using atomic absorption spectroscopy. The content of  $\text{Fe}^{2+}$  contained in the nanoparticles due to incomplete oxidation during synthesis was determined using chemical analysis to be below 2% of the total Fe (Makovec and Drofenik 2008).

The specific magnetization of the samples was measured using a Lake Shore 7312 vibrating-sample magnetometer.

The local structure in the neighborhood of the constituent cations in the nanoparticles was studied by X-ray absorption spectroscopy. The samples for XAFS analysis were prepared by mixing the nanoparticles with boron nitride and pressing the mixture into thin

homogeneous pellets. The absorption thickness of a pellet was about 1.5 above Fe or Zn K-edge absorption edge. EXAFS spectra at the K-edges of the metals were measured in a standard transmission mode at the C station of HASYLAB synchrotron facility, DESY (Hamburg, Germany). A Si(111) double-crystal monochromator was used with 1 eV resolution at 7 keV. Harmonics were effectively eliminated by detuning the monochromator crystal using a stabilization feedback control. The three ionization detectors were filled with 140 mbar Ar, 900 mbar Ar, and 900 mbar Ar. Sample pellets were placed between the first two detectors. The exact energy calibration with a precision of 0.05 eV was established with a simultaneous absorption measurement on the corresponding (Zn or Fe) metal foil placed between the second and the third ionization detector.

The absorption spectra were measured within the interval from -250 to 1000 eV relative to the K-edge of the constituent metal. In the XANES region, equidistant energy steps of 0.25 eV were used for a precise determination of the edge shape and position, while for the EXAFS region equidistant k-steps ( $\Delta k \approx 0.03 \text{ \AA}^{-1}$ ) were adopted with an integration time of 2 s/step. The positions of both Zn and Fe edges were, within experimental error, the same for all samples.

The spectra were analyzed with the IFEFFIT code (Ravel and Newville 2005; Rehr et al. 1992). The FEFF model of the EXAFS signal at the two metal K-edges was built from the crystallographic data on the spinel ferrite (Koenig and Chol 1968). Following the argumentation in the study of Calvin (Calvin et al. 2002), a simultaneous relaxation of the two spectra of

a sample was performed, exploiting connections and restraints between the parameters of the FEFF models of the constituent elements. The advantage of this approach, with regard to the separate fitting of individual EXAFS signals, lies in a better statistical reliability of the determined structural parameters.

## Results and discussion

Figure 1 shows the diffraction patterns for the studied nanoparticles. Even when the composition differed considerably from the stoichiometric value, the diffraction patterns contained only the peaks that can be ascribed to the spinel structure. Note that large deviations in the composition of the Zn-ferrite bulk material from its stoichiometric value  $Zn/Fe = 0.5$  are not possible (Makovec and Drofenik 2008). The diffraction peaks are considerably narrower in the nanoparticles ZF0.5-8 than in the nanoparticles ZF0.5-3, and the peaks become even sharper with annealing. The particle size estimated from the broadening of the diffraction peaks is listed in Table 1. Depending on the conditions of the synthesis, the nanoparticle size was 3.2 nm in the sample ZF0.5-3, whereas for the nanoparticles ZFxx-8 the size slightly varied with the composition; but stayed close to 8 nm (Table 1). With annealing, the nanoparticles ZF0.5-8 started to grow above 180 °C, reaching 13.7 nm at 405 °C and 24.2 nm at 500 °C.

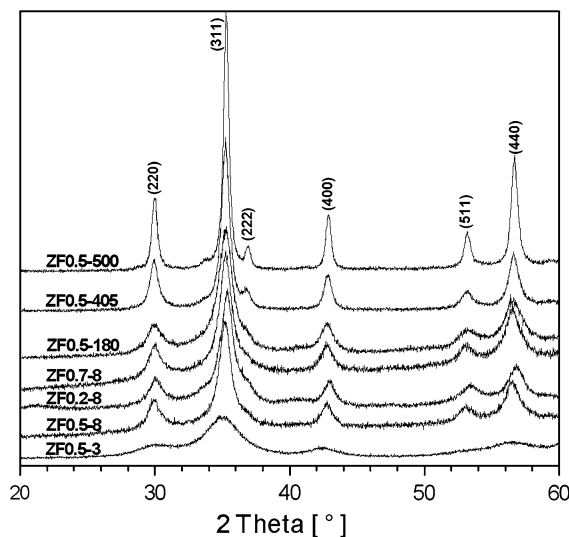


**Fig. 1** XRD spectra of the zinc-ferrite nanoparticles

The XRD size estimates agreed well with direct observations using TEM (Fig. 2). The nanoparticles retained a relatively narrow size distribution even after annealing. High-resolution electron microscopy showed good crystallinity of the nanoparticles.

The lattice parameter determined on the stoichiometric nanoparticles ZF0.5-8 ( $a = 0.8456$  nm) was significantly larger than that reported for  $ZnFe_2O_4$  bulk material ( $a = 0.8443$  nm) (Powder Diffraction File Card No. 89-4926, Joint Committee on Powder Diffraction Standards, Swerthmore, PA, 1984), suggesting a different crystalline structure. With the annealing, the cell parameter of the stoichiometric nanoparticles changed from the “nano” value at 180 °C ( $a = 0.8458$  nm) to the “bulk” value at 405 °C ( $a = 0.8441$  nm). In agreement with the larger size of  $Zn^{2+}$  ions compared to  $Fe^{3+}$  ions, the lattice parameter of the non-stoichiometric nanoparticles changed with their composition, from a larger value (0.8480 nm) for zinc-rich nanoparticles ZF0.7-8 ( $Zn/Fe = 0.71$ ) to a smaller value (0.8416 nm) for iron-rich nanoparticles ZF0.2-8 ( $Zn/Fe = 0.2$ ) outside the range of the stoichiometric nanoparticles.

The room-temperature measurements of specific magnetization as a function of magnetic field ( $M-H$ ) (Fig. 3) show ferrimagnetism for the as-synthesized zinc-ferrite nanoparticles and the nanoparticles annealed at 180 °C. Their magnetization hystereses show zero coercivity suggesting a superparamagnetic nature. As expected, specific magnetization (Table 1) was the highest for the Fe-rich nanoparticles ZF0.2-8, and the lowest for the Zn-rich nanoparticles ZF0.7-8. Also, the stoichiometric zinc-ferrite nanoparticles ZF0.5-0.3, ZF0.5-8, and ZF0.5-180 showed ferrimagnetism with significant specific magnetization indicating a partially inverted spinel structure. After annealing the stoichiometric nanoparticles at 405 and 500 °C, their structure rearranged to approach the normal-spinel bulk structure, and they became paramagnetic.

The nanoparticles were characterized using X-ray absorption spectroscopy. Neither Zn nor Fe EXAFS spectra showed any energy shift of the absorption edge that would suggest a change in the oxidation state. XANES analysis showed the nominal Fe(III) and Zn(II) valence. The local structure of the nanoparticles has been studied using EXAFS. The EXAFS of the nanoparticles of the different compositions were compared with the stoichiometric

**Fig. 2** TEM images and the corresponding particle size distribution of the as-synthesized nanoparticles ZF0.5-8 (**a, b**) and after annealing for 16 h at 500 °C in air (**c, d**)

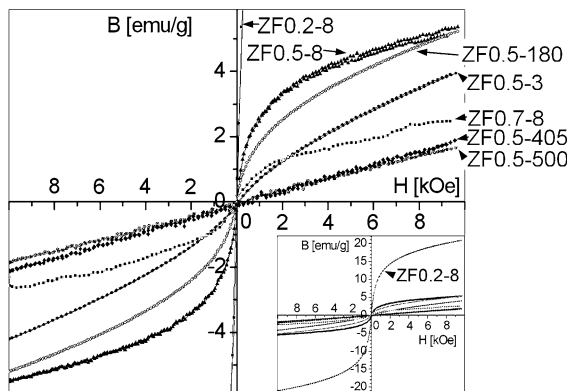
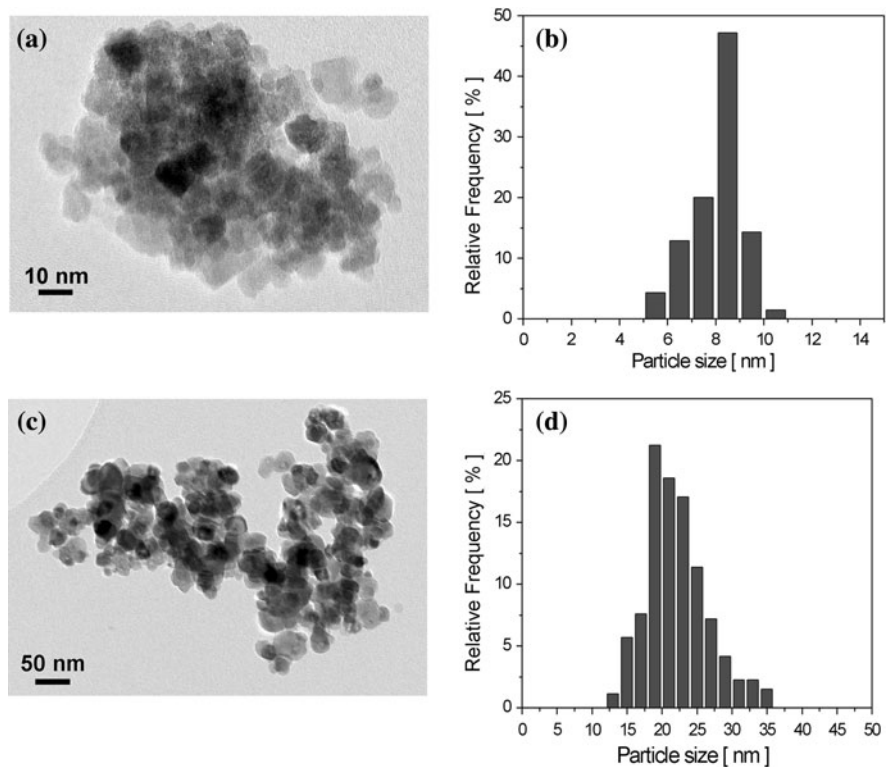
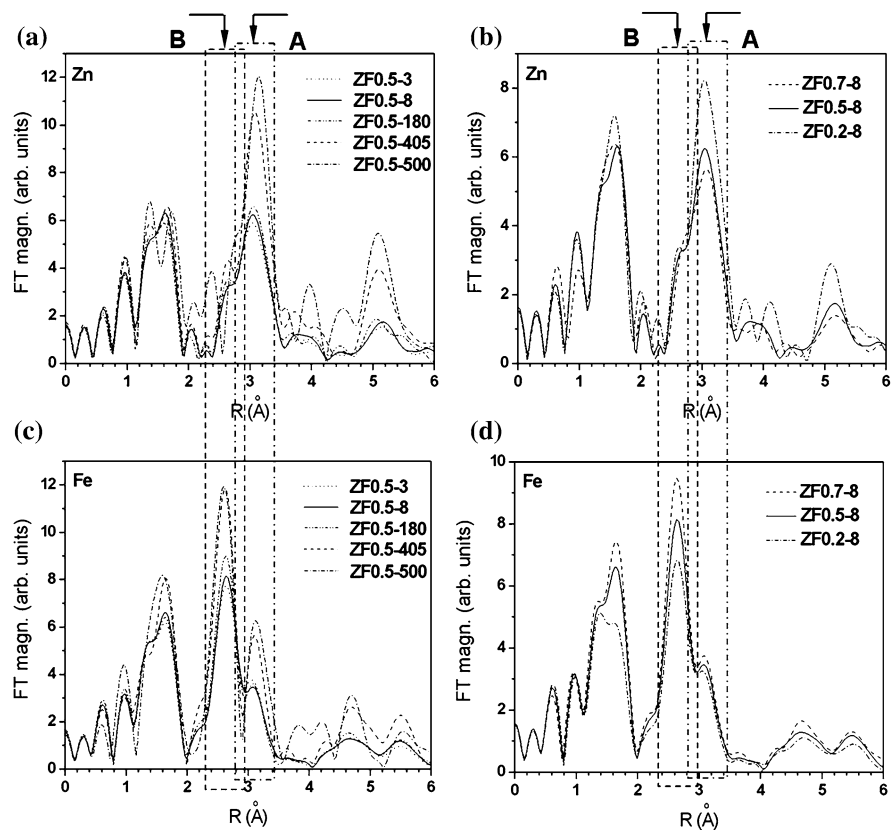


**Fig. 3** Room-temperature magnetization hysteresis of the zinc-ferrite nanoparticles

ZnFe<sub>2</sub>O<sub>4</sub> nanoparticles of different sizes. Some conclusions on the structure of the nanoparticles can already be made by inspection of the Fourier transforms of the EXAFS spectra shown in Fig. 4 (The  $k^2\chi(k)$  graphs are given in the supplement). The positions of the Fourier (FT) peaks, after a small phase correction, correspond to the bond distance between the absorbing and the backscattering atoms. The first peak in the FT EXAFS spectra around

~1.6 Å corresponds to oxygen ions comprising the oxygen polyhedra (The corresponding interatomic distance after phase correction is close to 2 Å). The amplitude of the first peak depends somewhat on the lattice site of the absorber cation, i.e., on the number of oxygen neighbors: it is larger for the octahedral sites (CN = 6) than for the tetrahedral sites (CN = 4). The scattering from the second neighbors forms the next wide peak in the FT EXAFS spectra, apparently composed of two components or subpeaks centered at ~2.6 Å and ~3.1 Å (corresponding to real distances of 3.0 and 3.6 Å, respectively). The relative amplitudes of those subpeaks depend strongly on the lattice site of the absorber cation. In spinel structure, the octahedral site has 6 s neighbors at the distance of 3.0 Å and 6 at the distance of 3.5 Å. The cation at a tetrahedral site has 12 s neighbors at the distance of 3.5 Å and 4 s neighbors at the distance of 3.6 Å. Thus, a subpeak in the FT EXAFS centered at ~2.6 Å (marked with B in Fig. 4) is contributed by the absorber cations incorporated at the octahedral sites, while the subpeak centered at 3.1 Å (marked with A) indicates the presence of the absorber cation at a tetrahedral lattice site.

**Fig. 4** FT EXAFS  $k^3$ -weighted spectra of Fe and Zn K-edge in the Zn-ferrite nanoparticles: **a** and **c** the spectra of the as-synthesized stoichiometric nanoparticles of two different sizes and the stoichiometric nanoparticles annealed at three different temperatures, **b** and **d** the spectra of the nanoparticles with different composition



In the FT EXAFS spectra of the as-synthesized and the annealed stoichiometric  $\text{ZnFe}_2\text{O}_4$  nanoparticles (Fig. 4a, c), two effects are clearly notable:

- (i) The amplitudes of the second-neighbor and further peaks increase with the increasing particle size. This effect shows that the average long-range crystalline order of the nanoparticles improves with the increasing size and the annealing temperature.
- (ii) The relative intensities of the sub-peaks A and B vary with the particle size suggesting swapping of Zn and Fe between the lattice sites with increasing annealing temperature. In the “bulk” state of the stoichiometric nanoparticles annealed at high temperatures above 400 °C, Zn EXAFS spectra show a prevalent A-subpeak, in agreement with the incorporation of Zn atoms predominantly at the tetrahedral sites. In the “nano” state of the as-synthesized nanoparticles or the nanoparticles annealed at 180 °C, the B-subpeak of significant amplitude suggests partial incorporation of Zn at the octahedral

sites. In the reverse trend, the Fe spectra show an increased proportion of the A-subpeak in the small nanoparticles.

While the partial migration of Zn ions from the tetrahedral sites to the octahedral sites with decrease in the nanoparticle size (compensated with the counter-migration of Fe ions) can be established already by a qualitative inspection of the EXAFS spectra, the interpretation of the EXAFS spectra of the nanoparticles of the different compositions (Fig. 4b, d) is not as straightforward.

In general, the non-stoichiometry can be structurally compensated in the bulk by adapted distribution of the cations over both sublattices of the spinel structure, or by formation of point defects. In the nanoparticles, the non-stoichiometry can also be compensated at the large surface area.

In the Fe-rich composition ZF0.2, the non-stoichiometry can theoretically be compensated in the bulk by either the vacancies or increased proportion of Fe at the A-sites. The compensation by A-site vacancies can be described by the structural formula

$(\text{Zn}_{0.4}(\text{V}_\text{A})_{0.6})[\text{Fe}_2]\text{O}_{3.4}(\text{V}_\text{O})_{0.6}$ , where round and square brackets represent tetrahedral (A) and octahedral [B] interstitial sites, respectively,  $\text{V}_\text{A}$  stands for A-sites vacancies, and  $\text{V}_\text{O}$  for oxygen vacancies. In the case of the incorporation of the increased proportion of Fe at the A-sites, cationic vacancies have to form for maintaining the overall charge neutrality (considering observed fixed oxidation state of the both cations). From the structure of maghemite ( $\gamma - \text{Fe}_2^{3+}\text{O}_3$ ), where the two-valent ion in the spinel structure is replaced with two-thirds of  $\text{Fe}^{3+}$  and one-third of vacancies at the B-positions— $(\text{Fe}^{3+})[\text{Fe}_{5/3}^{3+}(\text{V}_\text{B})_{1/3}]\text{O}_4$ —(Smit and Wijn 1959), it can be concluded that the B-site vacancies are energetically favorable over the A-site vacancies. Thus, the expected structural formula of the Fe-rich Zn-ferrite ZF0.5 with non-stoichiometry compensated in the bulk with increased proportion of Fe at the A-sites reads  $(\text{Zn}_{0.47}\text{Fe}_{0.53})[\text{Fe}_{1.82}(\text{V}_\text{B})_{0.18}]\text{O}_4$ . In the Zn-rich composition ZF0.7, the non-stoichiometry can theoretically be compensated in the bulk by the formation of the vacancies— $(\text{Zn}_1)[\text{Fe}_{1.43}(\text{V}_\text{B})_{0.47}]\text{O}_{3.15}(\text{V}_\text{O})_{0.85}$ —or by the incorporation of the “excess” Zn at the B-sites— $(\text{Zn}_1)[\text{Fe}_{1.77}\text{Zn}_{0.23}]\text{O}_{3.83}(\text{V}_\text{O})_{0.17}$ . Since the valence of  $\text{Zn}^{2+}$  is lower than that of  $\text{Fe}^{3+}$ , the charged oxygen vacancies have to form for the overall charge neutrality.

In the nanoparticles, both the non-stoichiometry itself, and the extra charge due to compensation of the non-stoichiometry in the bulk, can (partially) be compensated by surface effects. Already the surface termination of the nanoparticle with oxygen atoms or either kind of cations can result in a certain difference in the overall composition.

In order to determine the prevailing mechanism for the structural accommodation of the non-stoichiometry, the EXAFS spectra were modeled with an ab initio FEFF model (Ravel and Newville 2005).

The model was built from crystallographic data for cubic spinel (Koenig and Chol 1968), where the real coordinates of the neighbors around the target atom are defined with only two parameters, the isotropic expansion coefficient  $dr_0$  and the oxygen parameter  $p_\text{O}$ . The first was deduced from the XRD values of the lattice parameter in Table 1 and the second was fixed at the value 0.3842, the average of preliminary fits. For either metal, the model comprises two sets of scattering paths, one for each lattice site, within the range of 3.75 Å. The direct-scattering contributions

of two shells of oxygen neighbors and two shells (B- and A-sites) of metal neighbors are included, each site populated with either metal. The contribution of multiple-scattering paths within the range is negligible. The paths are described with standard EXAFS parameters: the lengths are adopted from the crystallographic data with a single free parameter  $dr_0$ , and the Debye–Waller widths of the distribution of the interatomic distances. The occupation probabilities of the two metals for the sites A and B ( $\text{Zn}_\text{A}$ ,  $\text{Zn}_\text{B}$ ,  $\text{Fe}_\text{A}$ , and  $\text{Fe}_\text{B}$ ) can be, taking into account the stoichiometric constraints, reduced to a single parameter, with additional parameters  $\text{V}_\text{A}$  and  $\text{V}_\text{B}$  describing the relative concentration of site vacancies. The concentration  $\text{V}_\text{A}$  was found negligible in preliminary tests. In order to detect the presence of oxygen vacancies, a parameter  $q_\text{O}$  is introduced as O-site occupation probability, with expected value of 1 in a normal structure. The intrinsic EXAFS parameters of photoelectron coherence fraction  $S_0^2$  for Fe and Zn were adopted from earlier analyses of similar materials, and the photoelectron zero energy correction  $E_0$  of the two metals from preliminary runs.

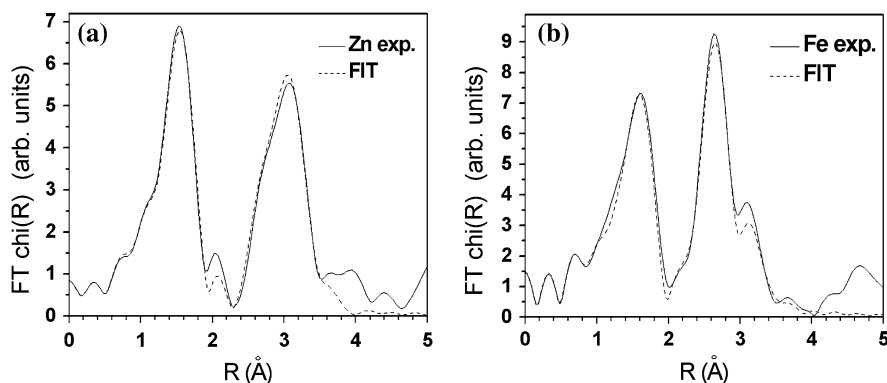
The best-fit structural parameters, obtained in a simultaneous fit in the  $k$ -range 3.6–12.8 Å<sup>−1</sup> for Fe and 4.4–11.9 Å<sup>−1</sup> for Zn, are given in Table 2 for all samples. In Fig. 5, the results of the least-square relaxation of the EXAFS spectra of the sample ZF07-8 to the model are shown. The quality of the fit is shown by the conventional EXAFS measure of  $r$ -factor, in the bottom row of the table. The bracketed values of the relative expansion  $dr_0$  are those adopted from the XRD lattice parameters while those in both the end columns were determined by the fit. They show a moderate expansion of the lattice for the increased disorder either in very small particles or in strong deviation from the stoichiometry. A similar effect of the disorder is found in the Debye–Waller widths  $\sigma^2$  of the typical metal–oxygen and metal–metal bond lengths. The oxygen occupation parameter  $q_\text{O}$  remains consistently in a narrow interval, albeit above the expected value of 1. Apparently, it compensates for some other small disregarded effect: if the values are renormalized to the average value 1.13 of the stoichiometric samples, some expected decrease for the Zn-rich sample ZF0.7-8 is found. A similar low value in the annealed sample ZF0.5-500 may be connected with the slight fluctuation with the cation vacancy concentration  $\text{V}_\text{B}$ .

**Table 2** The best-fit structural parameters, obtained in a simultaneous fit of Fe and Zn EXAFS spectra

	ZF0.5-3	ZF0.5-8	ZF0.5-180	ZF0.5-405	ZF0.5-500	ZF0.2-8	ZF0.7-8
Fe <sub>A</sub> [%]	12	9	10	8	2.6	23	0
Zn <sub>B</sub> [%]	23	17	19	16	4.8	0.7	30
V <sub>B</sub> [%]	4.0	2.3	0.	0.	1.3	22	0
$q_O$	1.15	1.13	1.13	1.13	1.10	1.15	1.11
$dr_0$	-0.0036	[-0.0049]	[-0.0047]	[-0.0067]	[-0.0068]	[-0.0096]	-0.0031
$\sigma_{(Fe-O)}^2 [\text{\AA}^2]$	0.0087	0.0079	0.0083	0.0068	0.0050	0.0100	0.0074
$\sigma_{(Fe-Fe)}^2 [\text{\AA}^2]$	0.0083	0.0082	0.0076	0.0055	0.0055	0.0088	0.0083
r-factor	0.024	0.021	0.018	0.018	0.033	0.025	0.021

$Fe_A$  the percentage of all Fe, found on A-site,  $Zn_B$  the percentage of Zn, found on B-site,  $V_B$  the percentage of vacancies at B-sites (taking into account two B-sites per formula unit),  $q_O$  the oxygen occupation probability,  $dr_0$  the relative correction to the crystallographic lengths in the model (with bracketed values adopted from the XRD lattice parameters),  $\sigma^2$  Debye–Waller widths of respective bond lengths

**Fig. 5** FT magnitude of the  $k^3$ -weighted Zn (a) and Fe (b) EXAFS data (solid line) with the model (dashed) for the sample ZF0.7-8. The background spline coefficients are relaxed together with the model parameters to improve the fit of the first-neighbor peak



The main discussion, however, is devoted to the site occupation probabilities. In the as-synthesized stoichiometric nanoparticles ZF0.5-8, the expected swapping of the Zn and Fe atoms between both the sublattices is evident. The degree of inversion increases strongly with decreasing nanoparticle size, from approximately 5% in the nanoparticles annealed at 500 °C (~24 nm in size) to 24% for the smallest nanoparticle (~3 nm). The modeling suggests the presence of the vacancies at the B-sites ( $V_B$ ) in the both as-synthesized stoichiometric nanoparticles, whereas with annealing the vacancies seem to disappear. Anyway, the content of  $V_B$  is relatively small in all the stoichiometric nanoparticles.

The swapping of the two ions between the two lattices of the spinel structure determined in the EXAFS analysis is generally well in accordance with magnetic properties of the stoichiometric nanoparticles (Fig. 3). Especially interesting is the sample

annealed at 405 °C, for which the modeling shows a significant degree of inversion of ~0.08, typical for the nanoparticles, and the paramagnetic nature, typical for the bulk. In order to exhibit ferrimagnetism, a significant proportion of the magnetic Fe ions has to be present at the A-sublattice together with nonmagnetic Zn to induce the super-exchange interactions and the ordering of magnetic spins. The small degree of inversion ( $x \sim 0.04$ ) present in the bulk  $ZnFe_2O_4$  (Ligenza 1976; O'Neill 1992) or in the nanoparticles annealed at 500 °C ( $x \sim 0.05$ ), and even much higher inversion in the nanoparticles annealed at 405 °C ( $x \sim 0.16$ ) is obviously too low to turn material ferrimagnetic. Since the stoichiometric 8-nm nanoparticles with  $x \sim 0.18$  are ferrimagnetic, it can be concluded that between 16 and 18% of Zn in the A-sublattice should be exchanged with magnetic Fe to induce the ferromagnetic ordering of the magnetic moments.

The EXAFS model proves that the non-stoichiometry in the nanoparticles is structurally accommodated predominantly by the structural changes in their cores and not merely by surface effects. The accommodation of non-stoichiometry is established by the adapted distribution of the cations over both the sublattices. The point defects are formed mainly for the compensation of the charge difference posed with non-stoichiometric compositions.

According to modeling, the stoichiometric 8-nm particles can be described with structural formula  $(\text{Zn}_{0.83}\text{Fe}_{0.18})[\text{Fe}_{1.82}\text{Zn}_{0.17}(\text{V}_\text{B})_{0.02}]\text{O}_{4-\delta}$  ( $\delta$ —possible oxygen non-stoichiometry—the modeling did not succeed in determining the absolute proportion of the oxygen vacancies). In the Fe-rich nanoparticles ZF0.2-8 of the comparable size, the excess proportion of Fe is incorporated at the A-sites and the proportion of  $\text{V}_\text{B}$  is increased for the compensation of the extra charge  $((\text{Zn}_{0.83}\text{Fe}_{0.18})[\text{Fe}_{1.82}\text{Zn}_{0.17}(\text{V}_\text{B})_{0.02}]\text{O}_{4-\delta})$ . In the Zn-rich nanoparticles ZF0.7-8, the A-sublattice is completely occupied by Zn and the additional proportion of Zn enters at B-sites. The model estimate of the proportion of Zn at the B-sites (30%) is even somewhat excessive. The partial exchange of  $\text{Fe}^{3+}$  at the B-sites with  $\text{Zn}^{2+}$  implies formation of oxygen vacancies for the charge compensation. The modeling shows a lower  $q_\text{O}$  value as compared to the Fe-rich nanoparticles, where no oxygen vacancies are expected.

## Conclusions

Contrary to the bulk, the zinc-ferrite nanoparticles with highly non-stoichiometric composition can be prepared without losing the single-phase spinel structure. The structural mechanisms enabling this non-stoichiometry were studied using the X-ray absorption fine structure (EXAFS) in the combination with X-ray diffractometry (XRD), transmission electron microscopy (TEM), and magnetic measurements. The nanoparticles were synthesized using co-precipitation in water-in-oil microemulsions. The modeling of the EXAFS spectra showed a significant degree of inversion  $x$   $((\text{Zn}_{1-x}\text{Fe}_x)[\text{Fe}_{2-x}\text{Zn}_x]\text{O}_4)$  already in the stoichiometric nanoparticles ( $\text{Zn}/\text{Fe} = 0.5$ ), resulting in their ferrimagnetic nature. The value of  $x$  decreases with increasing nanoparticles' size ( $x \sim 0.24$  for the nanoparticles with the

Scherer size of 3.2 nm, and  $x \sim 0.18$  for the size of 8 nm). With annealing, the value of  $x$  further gradually decreases as the nanoparticles grow, to reach the “bulk” value at approximately 500 °C. The flexibility in the structure of the nanoparticles enabled by swapping of the both cations between the two sublattices of the spinel structure is the dominant structural mechanism allowing high non-stoichiometry of the nanoparticles. In the Fe-rich zinc-ferrite nanoparticles ( $\text{Zn}/\text{Fe} = 0.2$ ), the extra proportion of Fe is incorporated at the A-sites while the vacancies are formed at the B-sites maintaining the charge balance. In the Zn-rich zinc-ferrite nanoparticles ( $\text{Zn}/\text{Fe} = 0.7$ ), the extra proportion of Zn enters the spinel structure at the B-sites.

**Acknowledgments** This study was supported by the Slovenian Research Agency, the Ministry of Higher Education, Science and Technology of the Republic of Slovenia within the National Research Program, and by DESY and the European Community under Contract RI13-CT-2004-506008 (IA-SFS). Provision of synchrotron radiation facilities by HASYLAB (project II-04-065 EC) is acknowledged. The authors would also like to thank Sašo Gyergyek for help with the magnetic measurements and E. Welter of HASYLAB for expert advice on beamline operation.

## References

- Ammar S, Jouini N, Fievet F, Stephan O, Marhic C, Richard M, Villain F, Chartier dit Moulin Ch, Brice S, Sainctavit Ph (2004) Influence of the synthesis parameters on the cation distribution of  $\text{ZnFe}_2\text{O}_4$  nanoparticles obtained by forced hydrolysis in polyol medium. *J Non Cryst Solids* 345 & 346:658–662
- Brockhouse BN, Corliss LM, Hastings JM (1955) Multiple scattering of slow neutrons by flat specimen and magnetic scattering by zinc ferrite. *Phys Rev* 98:1721–1727
- Calvin S, Carpenter EE, Ravel B, Harris VG, Morrison SA (2002) Multiedge refinement of extended x-ray absorption fine structure of manganese zinc ferrite nanoparticles. *Phys Rev B* 66:224405-1–224405-13
- Hamdeh HH, Ho JC, Oliver SA, Willey RJ, Oliveri G, Busca GJ (1997) Magnetic properties of partially-inverted zinc ferrite aerogel powders. *Appl Phys* 81:1851–1857
- Jeyadevan B, Tohji T, Nakatsuka KJ (1994) Structure-analysis of coprecipitated  $\text{ZnFe}_2\text{O}_4$  by extended X-ray absorption fine-structure. *Appl Phys* 76:6325–6327
- Kamiyama T, Haneda K, Sato T, Ikeda S, Asano H (1992) Cation distribution in  $\text{ZnFe}_2\text{O}_4$  fine particles studied by neutron powder diffraction. *Solid State Commun* 81:563–566
- Koenig U, Chol G (1968) Roentgenbeugungs- und Neutronenbeugungsuntersuchungen an Ferriten der Reihe  $\text{Mn}_x\text{Zn}_{1-x}\text{Fe}_2\text{O}_4$ . *J Appl Cryst* 1:124–126

- Ligenza S (1976) Study of spin interaction in manganese-substituted zinc ferrite by neutron spectroscopy. *Phys Stat Solidi (B)* 75:301–310
- Lotgering FK (1966) The influence of  $\text{Fe}^{3+}$  ions at tetrahedral sites on the magnetic properties of  $\text{ZnFe}_2\text{O}_4$ . *J Phys Chem Solids* 27:139–145
- Lykasov AA, D'yachuk VV, Pavlovskaya MS (1991) Univar- iant equilibria in Fe–Zn–O system. *Neorg Mater* 27:2153– 2157; *Inorg Mater* 27:446–449
- Makovec D, Drofenik M (2008) Non-stoichiometric zinc- ferrite spinel nanoparticles. *J Nanopart Res* 10:131–141
- Mason B (1947) Mineralogical aspects of the system  $\text{Fe}_3\text{O}_4$ –  $\text{Mn}_3\text{O}_4$ – $\text{ZnMn}_2\text{O}_4$ – $\text{ZnFe}_2\text{O}_4$ . *Am Miner* 32:426–432
- O'Neill HS (1992) Temperature-dependence of the cation distribution in zinc ferrite ( $\text{ZnFe}_2\text{O}_4$ ) from powder XRD structural refinement. *Eur J Miner* 4:571–580
- Ravel B, Newville M (2005) ATHENA, ARTEMIS, HEPHAESTUS: data analysis for X-ray absorption spectroscopy using IFEFFIT. *J Synchrotron Radiat* 12: 537–541
- Rehr JJ, Albers RC, Zabinsky SI (1992) High-order multiple- scattering calculations of X-ray-absorption fine-structure. *Phys Rev Lett* 69:3397–3400
- Sato T, Haneda K, Seki M, Iijima T (1990) Morphology and magnetic properties of ultrafine  $\text{ZnFe}_2\text{O}_4$  particles. *Appl Phys A50:13–16*
- Smit J, Wijn HPJ (1959) Ferrites. Philips' Technical Library, Eindhoven, The Netherlands
- Tanida K, Kitamura T (1984) System  $\text{Fe}_2\text{O}_3$ – $\text{ZnO}$ : subsolidus relations in air. *Tohoku Daigaku Senko Seiren Kenkyusho Iho* 40:71–76